

Feasibility Analysis, LCA and Demisability Tests of Wood-composites as Demisable and Eco-friendly Satellite Structures

Isil Sakraker-Özmen⁽¹⁾, Thomas Dauphin⁽¹⁾, Lars Wolfgramm⁽¹⁾, Clemens F. Kaiser⁽²⁾, Giovanni Piazza⁽³⁾, Michael Lengowski⁽²⁾, David B. Heyner⁽³⁾, Tom Spröwitz⁽⁴⁾, Georg Herdrich⁽²⁾

(1) Institute of Structures and Design, German Aerospace Center (DLR), Pfaffenwaldring 38-40, 70569 Stuttgart, Germany,

Isil.Sakraker@dlr.de; Thomas.Dauphin@dlr.de; Lars.Wolfgramm@dlr.de;

(2) Institute of Space Systems, University of Stuttgart, Pfaffenwaldring 29, 70569 Stuttgart, Germany
lengowski@irs.uni-stuttgart.de; kaiserc@irs.uni-stuttgart.de; herdrich@irs.uni-stuttgart.de

(3) Institute of Vehicle Concepts, German Aerospace Center (DLR), Pfaffenwaldring 38-40, 70569 Stuttgart, Germany

Giovanni.Piazza@dlr.de; David.Heyner@dlr.de

(4) Institute of Space Systems, German Aerospace Center (DLR), Robert-Hooke-Str. 7, 28359 Bremen, Germany
Tom.Sproewitz@dlr.de

ABSTRACT

The growing demand for space missions calls for more sustainable structural materials as the orbits become more crowded. This study evaluates Wood Aluminum Laminated Panels (WALP) as an environmentally friendly alternative to the conventional Aluminum Honeycomb Carbon Fiber Reinforced Plastic Panels (AHCP) used in satellite structures. First, a feasibility analysis was conducted for small satellite class (~100kg) and CubeSat platforms. Then a Life Cycle Assessment (LCA), focused on the Design and Production phases, following the European Space Agency's (ESA) EcoDesign framework, is performed. Finally, a plasma wind tunnel test was conducted for determining its demise behavior and assess the ablation products of the material for future evaluation of its effect on the atmosphere during its demise at re-entry.

1 INTRODUCTION

With increasing number of launches, especially to Low Earth Orbits (LEO), proactive approaches to mitigate space debris are essential to prevent scenarios like the Kessler Syndrome, where collisions lead to cascading debris. With satellite altitudes that are not too high, intentionally demising satellites into Earth's atmosphere is becoming increasingly attractive. However, this raises concerns about environmental impacts, such as increased metallic aerosols in the stratosphere, which affect the ozone layer and contribute to light pollution, impacting both terrestrial ecosystems and astronomical observations.

Correspondingly, innovative solutions to sustainable space exploration and protection of Earth's environment must be developed. This paper delves into wood-based materials for satellites which could reduce the

environmental impact during re-entry significantly and pose a first step towards eco-friendly satellite structures.

2 FEASIBILITY ANALYSIS

2.1 Material Description – DLR-FK

Environmentally friendly materials still must fulfill all requirements for spacecraft structures in order to substitute conventional ones. Important mechanical properties include the stiffness and strength of the material used so that they endure the launch and orbital loads. Additionally, special attention must be given to mass for space applications. Hence, according to Ashby, depending on the load conditions stiffness respectively strength is set in a certain relation to the density in order to determine performance indices (PI). These allow the comparison between different materials and the selection of the material that has the best ratio of mechanical value to its own weight for the individual load case. PI of woods can outperform classical used materials and are therefore considered for structural parts in this paper. [1]

Sandwich panels prove to be advantageous in reducing overall mass due to their structure consisting of a low-density core and high strength cover layers. While the cover layers are designed to be thin, the core takes up a large part of the overall wall thickness. A variety of lightweight materials can be used for the core as long as they can transmit compressive forces from cover layer to cover layer and handle normal flexural shear loads. Cores made of aluminum honeycomb or foam are standard in the aerospace industry. In other industries paper honeycomb, foams and light woods are also known. Cover layers can be made of thin metal sheets or of composite materials such as aramid or CFRP as long as they carry axial loads, bending moments, and in-plane shear loads. The bonding between the core and the cover

layers of the sandwich panel is achieved through an adhesive film. Due to the composition sandwich panels are anisotropic in their mechanical properties. Metallic or plastic inserts with treads or holes are glued into the core and used either to join two sandwich panels, to connect a panel to the rest of the structure, or to tighten components to the panel through regular fastening methods such as bolts, screws, rivets, or pins. [2]

Sandwich panels made of thin aluminum sheets with 0.6 mm thickness reinforced with plywood and a low-density wood core have already been designed and successfully tested at DLR for automotive industry [3]. A feasibility analysis for wood-based sandwich panels for aerospace industry is discussed in this paper. As natural raw material, woods have the following properties [4]:

- Orthotropic with three principal axes longitudinal (L) along the stem, radial (R) to the stem and transversal (T) to the radial direction
 - Mechanical properties of hardwoods: Young's Modulus: $E_L : E_T : E_R = 13 : 1.7 : 1$
Strengths in tension: $\sigma_L : \sigma_T : \sigma_R = 13 : 1.7 : 1$
 - Anisotropy in tension and compression with tensile to compressive strength in longitudinal direction: $\sigma_t : \sigma_c = 1.75 : 1$
 - Great variety of densities available throughout wood species with properties proportional to density and natural scatter in density and properties within same wood species
 - Properties depending on moisture content with lower moisture content resulting to higher moduli and strengths but lower elongation at break. Absorption respectively release of moisture leads to a change in the dimensions of the wooden parts (swelling and shrinking) possibly leading to cracks.
 - Properties depending on temperature with higher temperature leading to lower moduli and strengths.

Two woods are used for the specimens in this paper. One is balsa wood as there is no engineered material that offer a similar combination of mechanical properties and low density suitable for sandwich panel cores. The other being beech wood as it has high mechanical characteristics and is already used in structural applications but at the cost of a comparatively high density of 720 kg/m³.

Table 1 presents mechanical properties of commonly used materials in aerospace applications as well as of balsa and beech wood. [5]

Table 2 shows the derived PI according to Ashby. In theory, woods outperform classical used materials.

Table 1: Mechanical properties of commonly used metal materials in aerospace applications as well as wood

Material	Density ρ kg/m ³	Young's modulus E MPa	UTS σ MPa
Al 6061-T6	2700	68,000	275
Ti-6Al-4V	4400	110,000	825
CFRP (laminate)	1500	88,000	900
Balsa wood (L)	130	3,000	14
Beech wood (L)	720	14,400	105

Table 2: Comparison of PI for the bending of a plate

Material	PI stiffness of a plate $E^{1/3}/\rho$	PI strength of a plate $\sigma^{1/2}/\rho$
Al 6061-T6	15.1	6.1
Ti-6Al-4V	10.9	6.5
CFRP (laminate)	29.7	20.0
Balsa wood (L)	110.9	28.8
Beech wood (L)	33.8	14.2

High electrical conductivity in order to prevent statically charging and high thermal conductivity in order to prevent overheating are further requirements. A technical solution has to be found for woods as they are in general electrical insulators and heat-insulating materials. Lower density and lower moisture content increase both insulating effects. Table 3 presents key thermal and electrical properties of the discussed materials. [5]

Table 3: Electrical and thermal properties

Material	Electrical conductivity S/m	Thermal expansion $\mu\text{m}/(\text{m K})$	Thermal conductivity W/(m K)
Al 6061-T6	$2.5 \cdot 10^7$	23.6	167.00
Ti-6Al-4V	$5.8 \cdot 10^5$	9.0	6.70
CFRP (laminate)	$2.5 \cdot 10^3$	2.4	0.91
Balsa wood (L)	$1.0 \cdot 10^{-15}$	6.5	0.05
Beech wood (L)	$1.0 \cdot 10^{-15}$	6.0	0.48

Outgassing, the release of gases or volatiles from a material that were trapped, frozen, or absorbed, is induced into the materials when entering the vacuum environment in space. While structural issues arising from outgassing are unlikely, the subsequent deposition of the material can lead to chemical contamination, posing a hazard to both optical and electrically sensitive surfaces. Hence, outgassing of the moisture in wood must be examined and countermeasures taken if necessary.

From an economic point of view, wood is significantly cheaper than traditional lightweight construction materials.

Lastly, when taking sustainability into consideration, energy consumption of production and manufacturing processes for structural components as well as other environmental impacts such as acidification potential, eutrophication potential and human toxicity. In general, wood-based materials are significantly more sustainable in comparison to commonly used materials. [6]

2.2 Reference Cases and Simulations

In order to set a valid application framework for the wood composites, three different satellite classes were considered. A 3-unit CubeSat, a small satellite (Flying Laptop from Institute of Space Systems, IRS, of the University of Stuttgart) [7] and large satellite (Sentinel-2) were selected. For each satellite class, different structures were considered:

- CubeSat: Pure Wood laminates
- Small and Large Satellites: Aluminum-Wood-Aluminum Sandwich Structures

A total of 5 different concepts with different wood layups and geometries were considered. The launch load analysis conducted in ANSYS showed that the considered concepts was not suitable for the large satellites due to the very high sandwich thickness required. Due to the limited time, a limited reference case set of CubeSats and Small satellites were further developed. Figure 1 shows the concepts that were analyzed.



Figure 1: CubeSat concept of pure wood laminates (top) and small satellite concept with aluminum-wood sandwich structures (bottom).

2.3 Qualification Tests

Table 5 shows the summary of the conducted space qualification tests and simulations.

The thermal compliance was checked in the thermal vacuum chamber of the Space System Institute of University of Stuttgart. 9 cycles were successfully performed for three concepts between 10^{-3} – 10^{-4} mbar according to the ECSS-Q-ST-70-04C. The test setup can be seen in Figure 2.

Outgassing tests were performed at DLR Bremen facilities. The outgassing tests indicated non-compliance with ESA standards concerning Total Mass Loss (TML). This non-compliance is attributed to the expulsion of

water from the wooden material’s cellular structure under the low-pressure conditions of space. This can be overcome by applying acetylation process. And this is considered as the next future step in the feasibility analysis. New outgassing tests with the acetylated wood are planned after the submission date of this paper.

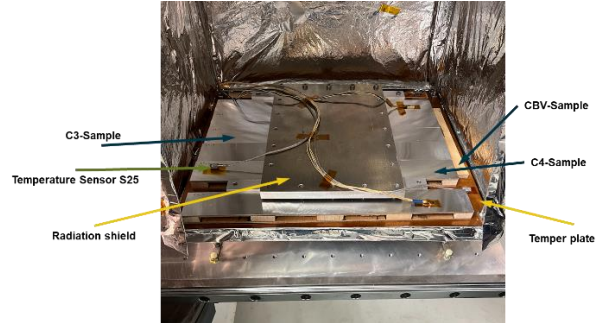


Figure 2: Thermal Vacuum Cycling Test setup prior to test.

Radiation shielding properties were checked with SPENVIS calculations as no budget could be allocated for radiation tests. 3 different orbits were considered, LEO, MEO and a GEO stationary orbit. For the wood aluminum sandwich panel, the shielding abilities were sufficient however for both types of pure wood, it was found that thicker material had to be used to achieve similar radiation properties with aluminum. The results are provided in Table 4.

Table 4: Radiation shielding properties calculated by SPENVIS for LEO, MEO and GEO respectively.

Parameter	Unit	Al.	Beech	Balsa
Density	kg/m ³	2700	750	110
Area-specific mass	kg/m ²	1.68	1.68	1.68
Thickness	mm	0.60	2.16	14.73
TID in LEO	krad	2.8	2.7	2.6
TID in MEO	krad	84.9	86.6	83.4
TID in GEO	krad	326.8	336.7	328.6

For electrical and atomic oxygen compliance no characterization tests could be performed within the analysis process. However, there are commercially available coatings, therefore it is not considered as a show-stopper. However, these two aspects will be considered in the Q3 of 2025.

2.4 Outcomes

Table 5 shows the summary of the conducted space qualification tests and simulations. While Large Satellites cannot be built by the investigated concepts, there are no insurmountable requirements expected for the 3-unit CubeSat or the Small Satellite. Nevertheless, further research is needed.

Table 5: Summary of the qualification tests and simulations.

	3U CubeSat	Small Satellite	Large Satellite
Structural Compliance	✓	✓	✗
Thermal Compliance	✓	✓	✓
Outgassing	✓ - Coating needed	✓ - Coating needed	✓ - Coating needed
Radiation Compliance	✓	✓	✓
Electrical Compliance	✓ - Coating needed	✓ - Coating needed	✓ - Coating needed
Atomic Oxygen Effects	✓ - Coating needed	✓ - Coating needed	✓ - Coating needed

3 LIFE CYCLE ANALYSIS AND COMPARISON TO STATE-OF-THE-ART CFRP-ALUMINUM SANDWICH

In this study we evaluated the environmental impact of the newly developed Wood Aluminum Laminated Panel (WALP) and we compared it to the conventional Aluminum Honeycomb Carbon Fiber Reinforced Plastic Panel (AHCP), using a Life Cycle Assessment (LCA) focusing on the Design and Production phase of ESA’s EcoDesign cycle.

3.1 Methodology

The LCA follows a cradle-to-gate approach, considering material extraction, processing, and manufacturing. Environmental indicators were selected based on ESA’s LCA guidelines, and results were normalized and weighted for comparability. Monte Carlo simulations (500 iterations) were conducted to evaluate uncertainty. The assessment was done in OpenLCA, using the Ecoinvent and ESA LCA databases. The LCA was performed within the framework of DLR project S3D.

3.2 Impact Assessment

Figure 3 shows the results of the comparative LCA. It is also worth checking the impact categories for the WALP in different life cycle phases.

The key findings can be summarized as follows:

- Overall Environmental Impact: WALP demonstrated 1.95 times lower environmental impact than AHCP.
- Global Warming Potential (GWP): WALP’s GWP was 1.89 times lower than AHCP, primarily due to the aluminum alloy production in AHCP.
- Ozone Depletion Potential: AHCP showed a 257 times higher impact than WALP, driven by

- carbon fiber production.
- Land Use Potential: WALP had an 11 times higher Land Use impact, attributed to balsa and beechwood veneer production.
- Office Work: Responsible for ~60% of the design phase impact, mainly from electricity consumption.
- Testing: Thermal vacuum chamber tests significantly contributed to impacts, though data limitations remain.

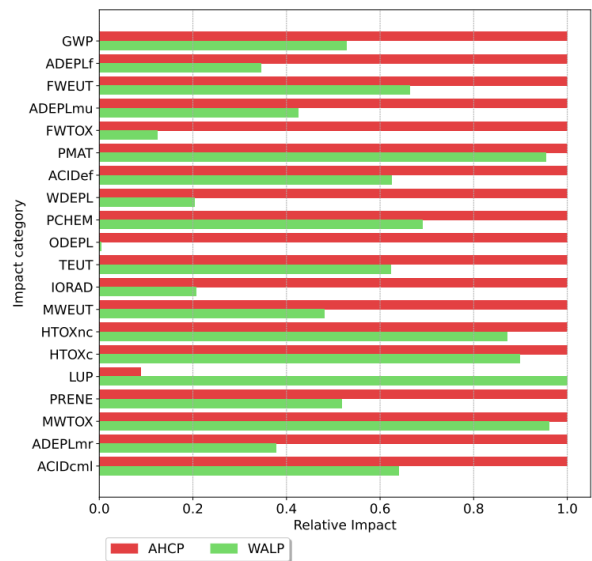


Figure 3: Overall impact comparison of the Aluminum Honeycomb CFRP Panels and the Wood Aluminum Laminated Panels.

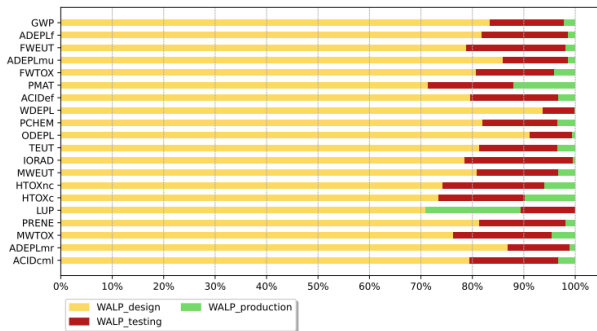


Figure 4: Design and Testing Phase Impacts of WALP.

3.3 Conclusion

WALP presents a viable, environmentally friendly alternative to AHCP, particularly in reducing carbon emissions and ozone depletion. Monte Carlo uncertainty analysis highlights data gaps, particularly for water depletion and human toxicity potential. The findings support WALP's potential as a sustainable structural alternative, emphasizing the need for enhanced data collection and collaboration within the space sector.

Next steps are applying LCA specific to the effects of the demise of WALP during re-entry, therefore the End-of-Life phase of ESA's EcoDesign cycle. Hence next chapter presents the data generation for this step by determining the ablation products. Furthermore, the social and economic impact analysis will also be performed in 2025 within S3D project.

4 DEMISABILITY TESTS IN PLASMA WIND TUNNEL – IRS

4.1 Plasma Wind Tunnel Test facility

The Institute of Space Systems (IRS) at the University of Stuttgart operates four PWT facilities which are used for re-entry investigations. The thermochemical loads at the stagnation point during re-entry can be replicated on the ground by creating a high-enthalpy air flow with a plasma generator in a vacuum chamber. For the presented study, PWK4 was used, which is equipped with the RB3 thermal arcjet plasma generator. A picture of the facility is shown in Figure 5. [7]

The 6-meter-long stainless-steel PWT tank with a diameter of 2 m is equipped with a 4-axis computerized numerical control (CNC) table onto which different probes can be mounted. A centralized direct current power supply for the plasma generator and a central multi-stage vacuum system are available at the IRS for PWT operations.

For characterizing the flow at the test condition, a heat flux/pitot double probe is used. A detailed description of the calorimetric heat flux measurement principle can be found in [8].



Figure 5. Image of the IRS PWK4 plasma wind tunnel facility.

A dedicated material probe is used to hold a 26.5 mm diameter coin type specimen in the center of the plasma beam. Figure 6. Shows a cross section of the probe head which is designed to thermally insulate the sample from the water-cooled structure of the probe foot. A cap made of sintered silicon carbide (SSiC) provides the ESA standard probe geometry.

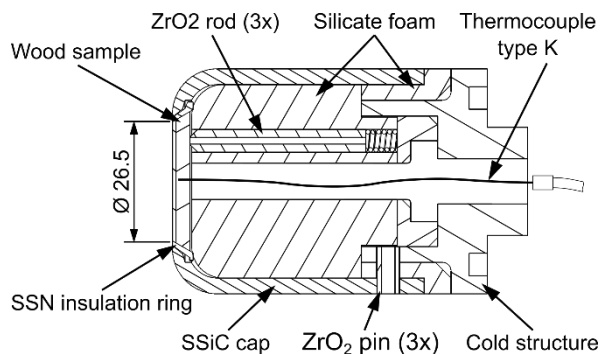


Figure 6. Cross section of the material probe for PWT experiments equipped with a type K thermocouple.

4.2 Test Conditions

The operating parameters of PWK4 and the characterized test conditions are stated in Tab. 6. The test position is set at $x = 160$ mm from the nozzle exit plane in the center of the plasma plume and the pressures depict a supersonic condition. The mass-specific enthalpy was determined according to the ASTM E637 standard [9], with assuming the fully catalytic heat flux being 1.25 times the reference heat flux on a cold copper oxide (CuO_x) surface [10].

The test conditions are representative of a LEO re-entry trajectory point at approximately 78 km with a velocity of 6940 m/s. This trajectory point was intensively investigated in the past and corresponds to the common break-up altitude suggested by the European Space Agency ESA [11].

Table 6. PWK4 operating parameters and test conditions.

Parameter	Unit	Value
Operating conditions		
Anode Current	[A]	650
Anode Voltage	[V]	90
Power	[kW]	58.5
Solenoid Current	[A]	100
Nitrogen mass flow rate	[g/s]	4.00
Oxygen mass flow rate	[g/s]	1.23
Ambient pressure	[Pa]	24
Arcjet plenum pressure	[hPa]	272
Conditions at the test position		
Ref. position x	[mm]	160
Ref. heat flux (CuO_x)	[kW/m ²]	803
Stagnation pressure	[Pa]	654
Mass-specific enthalpy	[MJ/kg]	24.1

4.3 Test Setup

The sample tested in the PWT is made of 1 mm beech veneer and approximately 3.5 mm balsa glued together with Araldite adhesive. Two different views (front and side) of the wood sample tested in the PWT are shown in Figure 7. The sample weight is 0.9215 g.



Figure 7. Pictures of the wood sample tested in PWK4.

For the PWT demise experiment, a type K thermocouple (TC) is pushed through the balsa in the center of the backside until it touches the beech veneer.

The setup of the demise experiment in PWK4 is shown in Figure 8. For contactless temperature measurements an LP3 linear pyrometer and a LumaSense MCS640 thermographic infrared camera are used. Both have a measurement wavelength of 960 nm where minimal disturbances by plasma radiation are present. The emissivity of the wood sample is assumed to be 0.80 [12] as it is charred immediately. Additionally, two Sony Alpha 6400 4K video cameras are used to document the demise process visually. An optical emission spectroscopy (OES) setup is employed to measure plasma radiation in the stagnation point region. It consists of an Ocean Optics HR4PRO-XR-ES USB spectrometer, a Thorlabs M112L02 fiber, an in-house built lens collimator with 88 mm focal length, and a Thorlabs

NDUV220B neutral density filter. The field of view has a diameter of approximately 5 mm.

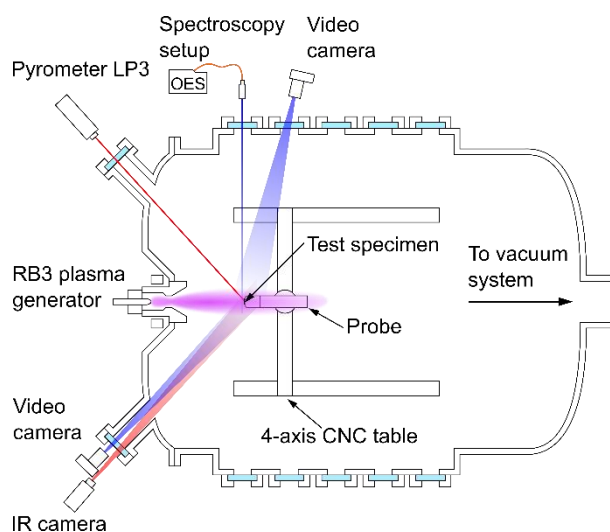


Figure 8. Experimental setup in PWK4.

Before the demise experiment begins, the sample is mounted on the material probe, the tank is evacuated, and the plasma generator is ignited. After the operating parameters are set, the sample is moved in lateral direction from a stand-by position 200 mm from the generator axis to the center of the plasma flow.

4.4 Plasma Wind Tunnel Test Results

The wood sample demised completely 29 seconds after being exposed to the high-enthalpy flow. Figure 9 shows pictures of the sample mounted in the material probe before and after the demise test. On the righthand side, only the insulator and zirconium oxide rods can be seen inside the SSiC cap as the sample is fully demised



Figure 9. Pictures of the material probe with the wood sample before (left) and after (right) the PWT test.

A picture of the material probe 10 seconds into the experiment is shown in Figure 10. On the right-hand side, the plasma plume exiting the generator can be seen. In the center of the image, the shock and bright boundary layer can be seen where especially carbonaceous species are emitting optical radiation.

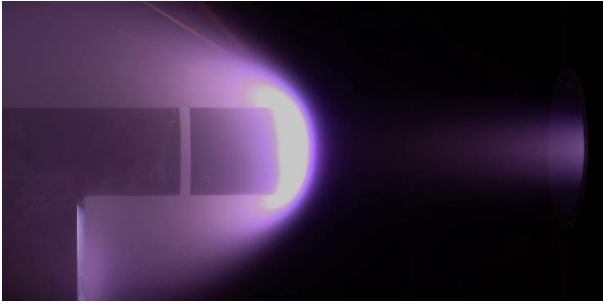


Figure 10. Picture of the material probe during the experiment from the side at $t = 10$ s.

Figure 11 shows the temperatures measured with the TC, the LP3 linear pyrometer, and the LumaSense thermographic camera. The measuring region of the LP3 is placed at the center of the sample and has a diameter of approximately 3 mm. Region of Interest (ROI) 1 of the LumaSense camera covers the whole surface of the sample while ROI2 is placed at its center. Additionally, thermographic images of the LumaSense camera at various points in time are shown in Figure 12.

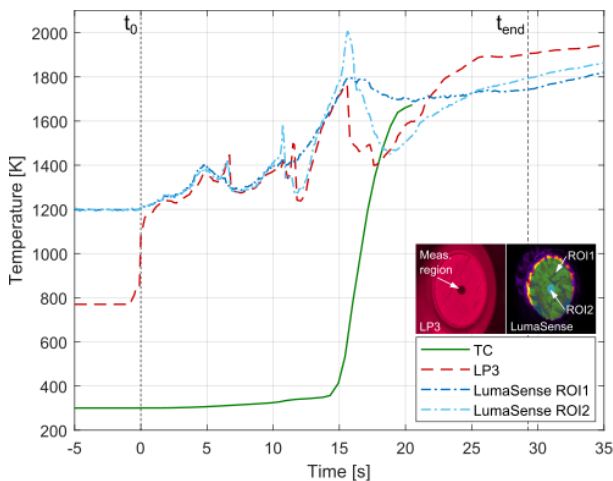


Figure 11. Temperature measurements with TC, LP3 linear pyrometer, and LumaSense thermographic camera. LP3 measuring region and LumaSense ROIs 1&2 marked on respective images.

Before the sample is moved to the test position in the center of the plasma plume at $t = 0$ s, the LP3 pyrometer and LumaSense camera read their minimum measurement temperature at approximately 770 K and 1200 K, respectively. When exposed to the plasma plume, the wood specimen quickly heats up above 1200 K. Wood fibers from the beech top layer are detaching from the surface and glowing at temperatures above 2000 K before being spalled. Spallation particles can be seen in Figure 10 as red traces above the material probe. Temperature peaks in the LP3 and LumaSense measurements are associated with hot fibers in their respective fields of view. After 10 seconds, the beech

veneer is ablated in the center of the sample resulting in the exposure of the balsa to the plasma flow. With the ablation of the veneer, the temperature in the balsa quickly rises, as the TC measurements indicate, which causes the balsa to expand. The surface temperature of the balsa reaches up to 1800 K, while the temperature of smaller balsa particles exceeds 2000 K. The balsa quickly decomposes and fragments are spalled into the flow. Since the specimen loses its structural integrity, the zirconium dioxide rods of the material probe are pushed through the sample after 16 seconds. After 29 seconds, the wood sample is completely demised.

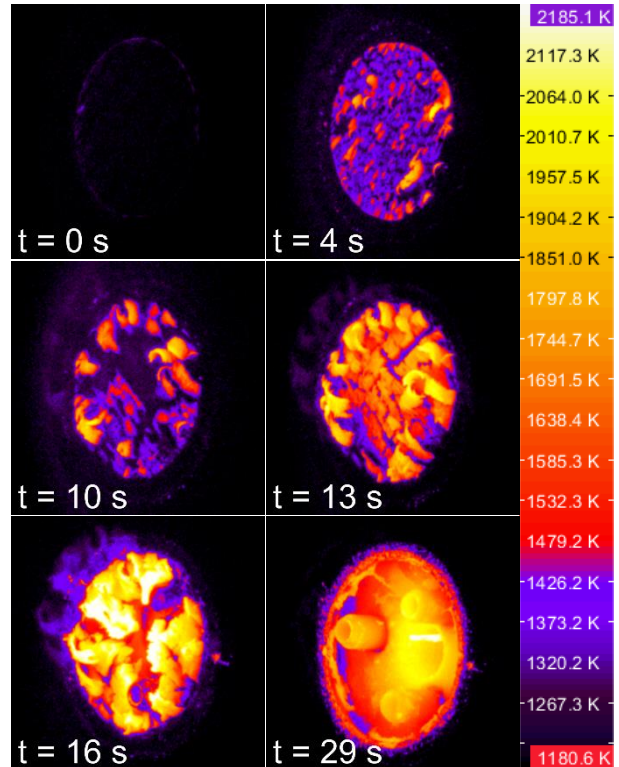


Figure 12. LumaSense thermographic images at various points in time throughout the experiment.

The OES measurement results are shown in Figure 13 and Figure 14. While the first image depicts the emitted spectral intensity over time and wavelength, the second image shows the spectral intensity over wavelength at two distinct points in time ($t = 5$ s & $t = 13$ s). With the beginning of the experiment, strong optical emission from CN molecules and moderate emissions from, CH, and C_2 molecules start immediately and intensify within the first seconds. Additionally, hydrogen (H), sodium (Na) and potassium (K) emissions can be seen next to emission from the air species nitrogen (N_2 , N) and oxygen (O). After the beech veneer is ablated, sodium and potassium emissions intensify (see Figure 14) which might stem from the adhesive or balsa wood. When the balsa heats up, it expands into the field of view of the spectroscopy setup. The thermal radiation from the hot

surface can be seen especially at higher wavelengths. The intensity reaches its maximum at approximately $t = 16$ s and decreases afterwards with the demise of the wood. The optical emissions, except for air plasma emissions, lose intensity in the following and diminish at the end of the experiment.

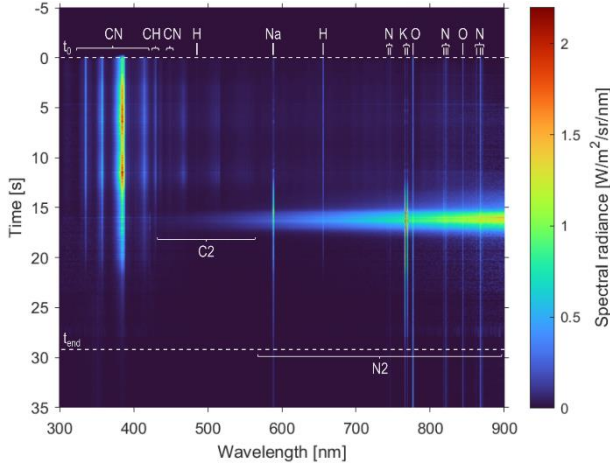


Figure 13. Optically emitted spectral radiance over time and wavelength.

The OES measurements at $t=5$ s and $t=13$ s reveal comparable intensities for carbonaceous species. However, the spectrum at $t = 13$ s, exhibits significantly higher intensities for sodium and potassium emissions, which can be attributed to the demise of balsa wood and Araldite. At wavelengths above 700 nm, the thermal radiation of the hot surface reaching into the OES field of view can be seen for the later point in time.

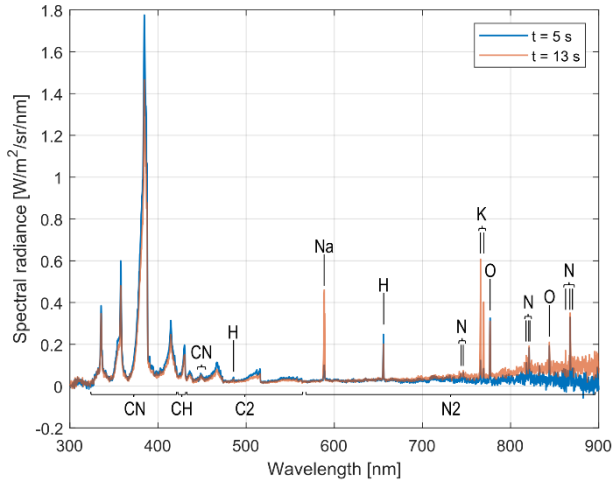


Figure 14. OES spectrum at $t = 5$ s and $t = 13$ s.

In order to compare the demisability of the tested wood sample to other materials, the effective heat of ablation $h_{abl,eff}$ is determined, which is defined as:

$$h_{abl,eff} = \frac{A_f}{m_0 - m_1} \cdot \int_{t_0}^{t_1} \dot{q}_{eff} dt. \quad (1)$$

Here, $A_f = 5.515$ cm² is the front surface area of the sample m_0 and m_1 are the masses of the sample at times t_0 and t_1 , respectively. In a holistic approach proposed by Sutton [13], the effective heat flux \dot{q}_{eff} is constant over time and assumed to be the fully catalytic heat flux $\dot{q}_{fc} = 1004$ kW/m². As the specimen completely demised in this experiment m_1 is zero, and $m_0 = 921.5$ mg is the initial mass of the sample. The duration of the experiment is $t_1 = 29$ s, for a complete demise of the sample, while the initial time is $t_1 = 0$ s. However, this potentially leads to an overestimation of the absorbed heat as the sample is already demised in the center at $t = 16$ s. When considering these two durations as upper and lower limits, the effective heat of ablation is in the range of 9.6 MJ/kg to 17.4 MJ/kg with an average value of 13.5 MJ/kg. Effective heats of ablation of 1.8 ± 0.8 MJ/kg for the AA7075 aluminum alloy and 98 MJ/kg for the pyrolysis and 45.0 ± 3 MJ/kg for the ablation of CFRP EX-1515 were determined [14].

4.5 Conclusion

A beech-balsa wood panel was exposed to a high-enthalpy flow relevant for LEO re-entry. The sample completely demised within 29 seconds at temperatures up to 2000 K. In the ablation process, CN, CH, C₂, as well as sodium and potassium emissions were detected with OES. To quantify the demisability of the sample, the effective heat of ablation was determined to be 13.5 ± 3.9 MJ/kg. Further investigations are necessary for a meaningful demisability comparison with other materials.

5 CONCLUSION AND OUTLOOK

Due to the increased metallic content onboard satellites and its negative effects on the atmosphere and the environment, wood-based materials were considered as an eco-friendly alternative. The feasibility of their use has been investigated for three satellite classes being CubeSat, small satellite and large satellites and two concepts were found feasible for CubeSats and small satellites: pure wood laminate panels and aluminum-wood sandwich structures. Extensive qualification tests and simulations were performed. Additionally, a life-cycle analysis has been done to compare the environmental impact indicators with CFRP-aluminum sandwich panels and wood sandwich panels were found to be less impactful. Finally, the demise behavior of the wood samples was tested in the plasma wind tunnel. It was shown that it is much more demisable compared to the state-of-the-art materials and the species produced during the ablation process were determined. This forms the baseline for further investigations of the effect of

wood demise on the atmosphere.

6 REFERENCES

- [1] M. F. Ashby, *Materials Selection in Mechanical Design*, 5th ed., Elsevier Science & Technology, 2016.
- [2] B. J. Kim and D. G. Lee, Characteristics of joining inserts for composite sandwich panels, *Composite Structures*, Volume 86, 2008.
- [3] G. Piazza and et al., *Innovative Holzanwendungen für die Mobilität der Zukunft*, Stuttgart: Cluster Innovativ am Holzbau-Donnerstag, 2023.
- [4] S. J., *Eigenschaften und kenngrößen von Holzarten*, Zürich: Baufachverlag Lignum beim hep Verlag, 1997.
- [5] T. Dauphin, *Feasibility Analysis on the Use of Wood-based*, Stuttgart: IRS-23-S-075, 2024.
- [6] S. Rütter and S. Diedrichs, *Ökobilanz-Basisdaten für Bauprodukte aus Holz*, unter, (zuletzt abgerufen am, <https://www.fnr.de/ftp/pdf/berichte/22028808.pdf>: last visited on 18.02.2025, 2012.
- [7] S. Klinkner, S. Gaisser, L. Keim, K. Klemich, M. Lengowski and U. Mohr, "U. Stuttgart University`s reliable, high-performance small satellite platform on its first mission "Flying Laptop", " in *IAA Symposium*, Berlin, 2019.
- [8] S. Loehle, F. Zander, M. Eberhart, T. A. Hermann, A. Meindl, B. Massuti-Bellester, D. Leiser, F. Hufgard, A. Pagan, G. Herdrich and S. Fasoulas, "The Plasma Wind Tunnels at the Institute of Space Systems: Current Status and Challenges," *CEAS Space Journal*, no. 14, pp. 395-406, 2022.
- [9] S. Loehle, A. Nawaz, G. Herdrich, S. Fasoulas, E. Martinez and G. Raiche, "Comparison of Heat Flux Gages for High Enthalpy Flows-NASA Ames and IRS," in *46th AIAA Thermophysics Conference*, 2016.
- [10] ASTM E637-05, "Standard Test Method for Calculation of Stagnation Enthalpy from Heat Transfer Theory and Experimental Measurements of Stagnation Point Heat Transfer and Pressure.," ASTM International, West Conshohocken, PA, 2005.
- [11] B. Massuti-Bellester, *Aerothermochemistry of High-Temperature Materials for Atmospheric Entry*, PhD Thesis, 2019.
- [12] European Space Research and Technology Center, "DIVE - Guidelines for Analysing and Testing the Demise of Man Made Space Objects During Re-entry," Noordwijk, Netherlands, 2020.
- [13] K. Ragland, D. Aerts and A. Baker, "Properties of wood for combustion analysis," *Bioresource technology*, vol. 37, no. 2, pp. 161-168, 1991.
- [14] G. W. Sutton, "The initial development of ablation heat protection, an historical perspective.," *Journal of Spacecraft and Rockets*, vol. 1, pp. 3-11, 1982.
- [15] A. S. Pagan and G. Herdrich, "Key Parameters Governing the Ground Risk from Reentering Pressure Vessel Debris," *Journal of Space Safety Engineering*, vol. 2, pp. 189-200, 2022.